

Traction force microscopy in *Dictyostelium* reveals distinct roles for myosin II motor and actin-crosslinking activity in polarized cell movement

Maria L. Lombardi¹, David A. Knecht¹, Micah Dembo² and Juliet Lee^{1,*}

¹Department of Molecular and Cell Biology, University of Connecticut, Storrs, CT 06269, USA

²Department of Biomedical Engineering, Boston University, Boston, MA 02215, USA

*Author for correspondence (e-mail: juliet.lee@uconn.edu)

Accepted 28 February 2007

Journal of Cell Science 120, 1624-1634 Published by The Company of Biologists 2007
doi:10.1242/jcs.002527

Summary

Continuous cell movement requires the coordination of protrusive forces at the leading edge with contractile forces at the rear of the cell. Myosin II is required to generate the necessary contractile force to facilitate retraction; however, *Dictyostelium* cells that lack myosin II (*mhcA*⁻) are still motile. To directly investigate the role of myosin II in contractility we used a gelatin traction force assay to measure the magnitude and dynamic redistribution of traction stresses generated by randomly moving wild-type, myosin II essential light chain null (*mlcE*⁻) and *mhcA*⁻ cells. Our data show that for each cell type, periods of rapid, directed cell movement occur when an asymmetrical distribution of traction stress is present, in which traction stresses at the rear are significantly higher than those at the front. We found that the major determinants of cell speed are the rate and frequency at which traction stress

asymmetry develops, not the absolute magnitude of traction stress. We conclude that traction stress asymmetry is important for rapid, polarized cell movement because high traction stresses at the rear promote retraction, whereas low traction at the front allows protrusion. We propose that myosin II motor activity increases the rate and frequency at which traction stress asymmetry develops, whereas actin crosslinking activity is important for stabilizing it.

Supplementary material available online at
<http://jcs.biologists.org/cgi/content/full/120/9/1624/DC1>

Key words: Traction forces, Myosin II, Myosin essential light chain, Movement, *Dictyostelium discoideum*

Introduction

It is generally accepted that cell movement requires the production of myosin-II-dependent contractile forces at the cell rear to induce retraction (Chen, 1981; Clow and McNally, 1999; Jay et al., 1995). This is supported by the finding that myosin II is localized to the rear of moving cells (Kolega, 2006; Rubino et al., 1984; Verkhovskiy et al., 1999; Yumura et al., 1984). However, myosin II heavy chain null (*mhcA*⁻) *Dictyostelium* cells are still able to move, albeit more slowly than wild-type cells (Wessels et al., 1988), indicating that myosin II activity may not be essential for *Dictyostelium* movement on glass. On more adhesive surfaces, the movement of myosin II null cells is dramatically reduced compared with the wild type, suggesting that myosin-II-dependent contractile forces are particularly important for retraction when the cell is well adhered to the substratum (Doolittle et al., 1995; Jay et al., 1995). In related studies, cells that lack the essential light chain of myosin II (*mlcE*⁻) were found to polarize and move normally during cAMP-induced chemotaxis (Chen et al., 1995), wild-type aggregation streams (Xu et al., 2001) and an under-agarose chemotaxis assay (Laevsky and Knecht, 2003). Although *mlcE*⁻ cells have little or no contractile activity (Xu et al., 2001), myosin II that lacks the essential light chain can still crosslink actin (Ho and Chisholm, 1997; Xu et al., 2001), thus maintaining cortical rigidity that might compensate for the

lack of myosin II motor activity (Laevsky and Knecht, 2003; Xu et al., 2001). This raises the question of whether myosin II actin crosslinking activity in *mlcE*⁻ cells can generate the same amount of force for retraction as wild-type cells. If true, then does the reduced speed of *mhcA*⁻ cells result from the lack of myosin II actin crosslinking activity, myosin II motor activity or a combination of both?

Traction force assays offer a means to approach these questions because information is provided about the size and location of contractile forces in relation to cell movement (Beningo and Wang, 2002). These assays generally consist of an elastic or flexible substratum that deforms in proportion to the magnitude of the traction forces exerted on it by a moving cell. Given the material properties of an elastic substratum, such as the Young's Modulus, it is possible to determine the magnitude and orientation of traction stresses at discrete points beneath the cell. In addition, the pattern of traction forces is related to the cell shape, speed and mode of movement (Dembo et al., 1996; Harris et al., 1980; Lee et al., 1994). Slow-moving cells (~0.5 μm/minute), such as fibroblasts, generate strong, inward facing traction forces (~20 kdynes/cm²) that are located predominately behind the leading edge, and are suggested to provide sufficient force to 'tow' the cell forward (Beningo et al., 2002; Dembo and Wang, 1999; Munevar et al., 2001). By contrast, rapidly moving fish epithelial keratocytes (~30

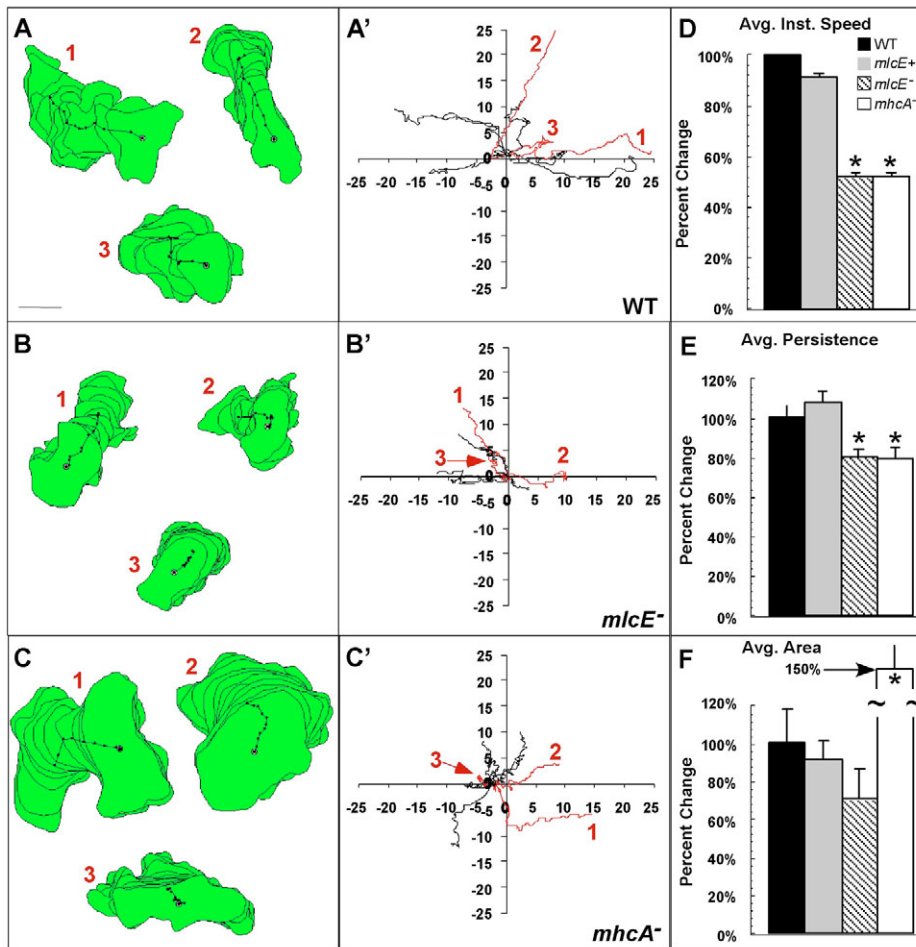


Fig. 1. The motile behavior of *Dictyostelium* moving on gelatin. (A-C) Stacked cell outlines, overlaid with a centroid track, from three representative cells of each type; wild-type, *mlcE*⁻ and *mhca*⁻ cells. Examples of cells moving randomly at fast (1), intermediate (2) and slow (3) speeds, for each cell type, over a ~3-minute period are shown. (A'-C') Rose plots, showing the total distance traveled and the directionality of movement for each cell type during a ~3-minute period. Bar, 5 μm . (D-F) Summary histograms of the mean relative changes in instantaneous speed (D), persistence (E) and spread area (F) with respect to the wild-type value that was set to 100% for wild-type (black bar), *mlcE*⁺ (gray bar), *mlcE*⁻ (striped bar) and *mhca*⁻ cells (open bar, $n=9$). Asterisks indicate statistically significant differences compared with wild-type cells ($P < 0.05$), using a Student's *t*-test, assuming unequal variances.

$\mu\text{m}/\text{minute}$) generate relatively weak traction forces (~ 2 kdynes/ cm^2), the largest of which are located at the lateral rear edges of the cell, where they facilitate retraction (Lee et al., 1994).

To detect the traction forces produced by rapidly moving cells the substratum must be highly sensitive to deformation. Examples of these include weakly crosslinked films of silicone (Burton et al., 1999; Lee et al., 1994; Oliver et al., 1998) and gelatin (Doyle and Lee, 2002). Recently, both wild-type and myosin II null *Dictyostelium* cells were found to deform weakly crosslinked silicone substrata (Uchida et al., 2003). However, the spatial resolution of silicone traction force assays is poor because of their low 'stress contrast' (Dembo and Wang, 1999; Marganski et al., 2003). This means that large traction stresses will 'overshadow' smaller ones, especially if they are close together, and it is likely to pose a problem for imaging traction stresses in small cell types like *Dictyostelium* with an average diameter of 10 μm . Gelatin substrata have a spatial resolution that is an order of magnitude greater than crosslinked silicone films, and are thus well suited for traction force microscopy (TFM) in *Dictyostelium*. Here we have used a gelatin traction force assay to detect the traction forces produced by wild-type, *mlcE*⁻ and *mhca*⁻ *Dictyostelium* and generated vector maps of the traction stresses produced by these cell types using custom traction mapping software, LIBTRC (Dembo and Wang, 1999; Marganski et al., 2003). We have correlated changes in the magnitude and distribution

of traction stresses with measures of cell speed, area and shape, during cycles of protrusion and retraction. We found that for each cell type, the most rapid movement occurred when an asymmetrical distribution of traction stress exists, in which forces at the rear are significantly greater than at the front, irrespective of the absolute value of traction stress magnitude. In addition we observed characteristic differences in the rate and extent to which traction stress asymmetry develops between cell types, which can be related to the distinct functions of myosin II motor and actin crosslinking activities.

Results

Motile behavior of randomly moving *Dictyostelium discoideum* on gelatin substrata

To characterize the motile behavior of *Dictyostelium* cells moving randomly on gelatin, we generated stacks of cell outlines using DIAS (Soll et al., 2003), which show changes in shape, distance traveled and directionality characteristic of each cell type (Fig. 1A-C). Rose plots were used to show the total distance moved and directionality of all cells examined (Fig. 1A'-C'). On gelatin, the instantaneous speed of the wild type is 1.20 ± 0.44 $\mu\text{m}/\text{minute}$ (mean \pm s.d., $n=9$) and in *mlcE*⁻ cells is 1.07 $\mu\text{m}/\text{minute}$ (Fig. 1D, Table 1) and the persistence of the wild type ($P=0.58$) and *mlcE*⁺ ($P=0.60$) are also similar (Fig. 1E). Fast-moving wild-type cells tend to be elongated in the direction of movement and more directed compared with slower-moving cells (compare cells 1 and 2 with cell 3, Fig.

Table 1. Average traction stress, speed and area associated with wild-type and mutant *Dictyostelium* cells

Cell number	Mean TS (dynes/cm ²)	Mean speed (μm/minute)	Mean area (μm ²)
WT			
1	2.83×10 ³	1.74	4.63×10 ⁻²
2	2.66×10 ³	1.54	6.59×10 ⁻²
3	5.82×10 ³	0.77	5.82×10 ⁻²
4	1.29×10 ⁴	1.62	8.28×10 ⁻²
5	5.30×10 ³	1.56	7.23×10 ⁻²
6	3.73×10 ³	0.81	5.66×10 ⁻²
7	1.67×10 ⁴	0.71	5.69×10 ⁻²
8	1.39×10 ⁴	0.70	5.56×10 ⁻²
9	1.41×10 ³	1.39	6.07×10 ⁻²
Mean±s.d.	7.25×10 ³ ±4.06×10 ³	1.13±0.44	6.17×10 ⁻² ±1.07×10 ⁻³
<i>mlcE</i> ⁺			
1	8.31×10 ³	1.15	6.51×10 ⁻²
2	6.48×10 ³	1.08	6.24×10 ⁻²
3	1.07×10 ³	0.72	6.83×10 ⁻²
4	4.42×10 ³	0.96	5.97×10 ⁻²
5	1.57×10 ³	1.27	6.06×10 ⁻²
6	1.10×10 ³	0.99	6.06×10 ⁻²
7	9.02×10 ²	0.83	5.60×10 ⁻²
8	1.20×10 ³	1.44	6.85×10 ⁻²
9	1.11×10 ⁴	1.19	4.59×10 ⁻²
Mean±s.d.	3.96×10 ³ ±3.83×10 ³	1.07±0.22	6.08×10 ⁻² ±6.92×10 ⁻³
<i>mlcE</i> ⁻			
1	2.74×10 ³	0.75	6.04×10 ⁻²
2	1.40×10 ³	0.54	3.92×10 ⁻²
3	1.08×10 ³	0.40	6.53×10 ⁻²
4	2.65×10 ³	0.79	4.18×10 ⁻²
5	1.97×10 ³	0.75	3.67×10 ⁻²
6	1.45×10 ³	0.27	4.31×10 ⁻²
7	9.25×10 ²	0.77	5.25×10 ⁻²
8	2.82×10 ³	0.84	7.03×10 ⁻²
9	5.81×10 ²	0.41	4.91×10 ⁻²
Mean±s.d.	2.66×10 ³ ±2.59×10 ³	0.61±0.21	5.09×10 ⁻² ±1.21×10 ⁻²
<i>mhcA</i> ⁻			
1	4.67×10 ²	1.01	1.17×10 ⁻¹
2	4.12×10 ²	0.68	1.75×10 ⁻¹
3	7.13×10 ²	0.38	8.17×10 ⁻²
4	5.23×10 ²	0.46	6.34×10 ⁻¹
5	1.71×10 ³	0.99	1.10×10 ⁻¹
6	6.77×10 ²	0.46	1.25×10 ⁻¹
7	2.99×10 ²	0.40	6.19×10 ⁻²
8	2.78×10 ²	0.99	6.66×10 ⁻²
9	1.79×10 ²	0.70	6.30×10 ⁻¹
Mean±s.d.	5.84×10 ² ±4.58×10 ³	0.62±0.27	2.22×10 ⁻¹ ±2.35×10 ⁻¹

1A,A'). In *mlcE*⁻ cells, which lack most or all contractile activity but possess actin crosslinking function, the mean instantaneous speed (0.61±0.21 μm/minute; *n*=9) and persistence, are significantly lower than in both wild-type and *mlcE*⁺ cells (*P*=0.47; Fig. 1B,B',D,E, Table 1). Similar values of cell speed (0.62 μm/minute) and persistence were found for *mhcA*⁻ cells that lack the myosin II heavy chain (*P*=0.45 compared with values in wild-type and *mlcE*⁺ cells; Fig. 1C,C',D,E, Table 1). In general, *mhcA*⁻ cells are not well polarized and their movement is much less directed when compared with the other cell types (Fig. 1C,C'). However, a striking feature of *mhcA*⁻ movement is the ability of a few cells to move as fast as some slower-moving wild-type cells (cells 1, 2 in Fig. 1C,C'). Another characteristic feature of *mhcA*⁻ cells is that their mean area (2.22×10⁻¹±2.35×10⁻¹ μm²) is significantly larger (Fig. 1C,F and Table 1) than wild-type (6.17×10⁻²±1.07×10⁻³ μm²), *mlcE*⁺ (6.08×10⁻²±6.92×10⁻³ μm²) or *mlcE*⁻ (5.09×10⁻²±1.21×10⁻² μm²) cells. These results demonstrate the role of myosin II crosslinking activity in maintaining cortical rigidity that normally restricts the spread area of moving wild-type and *mlcE*⁻ *Dictyostelium* cells.

Typical patterns of traction stress beneath wild-type and mutant *Dictyostelium* cells

Traction vector maps for all cell types show that traction stresses are oriented inward and perpendicular to the cell margin (Fig. 2). A representative traction map of a wild-type cell shows an asymmetrical distribution of traction stress magnitude, in which the high forces (defined as equal to or greater than the 90th percentile traction stress, 1.30×10⁴ dynes/cm²) are typically located in a crescent shape at the rear, while the lower forces (6.23×10² dynes/cm²) are found at the middle and front of the cell (Fig. 2A). On average, the range of traction stress in wild-type cells is 1.41×10³-16.7×10³ dynes/cm² (Table 1). A similar, less marked, asymmetry in traction stresses is seen in *mlcE*⁻ cells, where a region of high traction stress (4.11×10³ dynes/cm²) is found at the rear together with a region of low traction stress (6.23×10² dynes/cm²) at the middle and front of the cell. However, the average 90th percentile traction stress (2.66×10³±2.59×10³ dynes/cm², *n*=9) produced by *mlcE*⁻ cells is about three times less than those generated by wild-type cells (7.25×10³±5.68×10³ dynes/cm², *n*=9, Table 1). In addition,

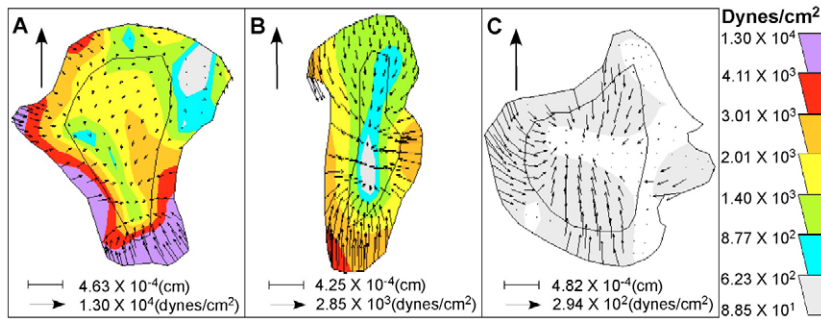


Fig. 2. Characteristic distribution of traction stress for wild-type, *mlcE*⁻ and *mhca*⁻ cells. Color-coded vector maps of the traction stresses generated by wild-type (A), *mlcE*⁻ (B), and *mhca*⁻ (C) cells, moving in the direction indicated (arrow). The length and orientation of arrows in the vector map represent the magnitude and direction of traction stresses. Note that the traction vector scale bar (horizontal arrow) in each map represents a traction stress that differs by approximately an order of magnitude between each cell type. Colored regions represent areas of traction stress within the same magnitude range. Areas of high (≥ 90 th percentile) traction stress are represented by red and purple colors, while areas of low traction stress are shown in gray, blue and light green.

the range of traction stress in *mlcE*⁻ cells is 0.58×10^3 – 9.25×10^3 dynes/cm² (Table 1). In contrast to wild-type and *mlcE*⁻ cells, the distribution of traction stress magnitude in *mhca*⁻ cells is more symmetrical (Fig. 2C). In addition, the 90th percentile traction stress for *mhca*⁻ cells is $5.84 \times 10^2 \pm 4.58 \times 10^2$ dynes/cm² (mean \pm s.d.; $n=9$) a value that is ~ 13 times less than in wild-type cells and ~ 4 times less than in *mlcE*⁻ cells. The range of traction stress in *mhca*⁻ cells is 0.179×10^3 – 1.71×10^3 dynes/cm² (Table 1).

An asymmetrical distribution of traction stress is associated with rapid movement in wild-type *Dictyostelium* cells

The movement of wild-type *Dictyostelium* is characterized by cycles of protrusion at the front cell edge and retraction at the rear. A corresponding series of traction maps shows the start of a cycle of movement as the development of a front-rear asymmetry in traction stress oriented in the direction of movement. The cycle ends following a retraction and loss of traction stress asymmetry. Protrusion may occur either simultaneously or following retraction. The average duration of one cycle of movement in wild-type cells is 25 ± 5 seconds (mean \pm s.d.; $n=12$, in nine cells). In all wild-type cells examined, higher traction stresses (red and purple regions) were found associated with retraction at the rear cell edge (Fig. 3A–C; see supplementary material, Movie 2), and protrusion occurred within regions of low traction stress (white to green regions) at the front of the cell (Fig. 3A–F). This asymmetrical distribution of traction stress is most pronounced prior to retraction and is regenerated while the cell is moving in a rapid, directed manner. In addition, cell shape shows the greatest degree of polarity during this time. In this example, a ‘crescent’ of high traction stress is seen at the rear that gradually decreases in size (Fig. 3A–C) then disappears as the rear detaches abruptly from the substratum (Fig. 3D). The cell rear undergoes what we term a ‘rapid recoil’ retraction, defined here as one that occurs on average within 5 ± 2 seconds (mean \pm s.d.;

$n=14$). This type of retraction is common in cells that appear to become stuck at the rear and thus show discrete phases of retraction and protrusion. Rapid recoil retractions are preceded by an increase in 90th percentile traction stress, whereas speed decreases and the cell elongates, giving it a stretched appearance (Fig. 3A–C,G). Once retraction (R), has occurred, traction stress decreases sharply and speed increases as the rear recoils towards the cell body (Fig. 3D–F,G). Retraction is also accompanied by a decrease in cell area and the cell becomes more rounded in shape (Fig. 3E,F,G). After retraction, a phase of protrusion begins, within regions of the lowest traction stress at the front of the cell (compare Fig. 3E with 3F).

Wild-type *Dictyostelium* cells that do not show discrete phases of protrusion and retraction exhibit a second mode of retraction that we refer to as a ‘slow recoil’ retraction, which take 30 ± 8 seconds to occur (mean \pm s.d.; $n=14$; Fig. 4, see supplementary material, Movie 3). In wild-type cells, 66% of all retractions are of the rapid recoil type, whereas 34% are slow recoil retractions. During this type of retraction, a region of high stress develops at the rear cell margin while a region of lower traction stress is found at the front edge (Fig. 4A–C). Unlike a rapid recoil retraction, slow recoil retractions proceed more slowly and occur simultaneously with protrusion (Fig. 4C–G). Prior to retraction, traction stress and speed increase together with a small increase in cell roundness but little change in cell area (Fig. 4A–C,M). During retraction (R) traction stress decreases, followed shortly by a decrease in cell speed (Fig. 4C–G,M). There is no significant change in cell shape but cell area decreases slightly (Fig. 4M). The magnitude of changes in traction stress, speed, cell area and shape are smaller and more gradual than in rapid recoil retractions.

Development of traction stress asymmetry is impaired in *mlcE*⁻ cells

Moving *mlcE*⁻ cells produce an asymmetrical distribution of traction stress, which although similar to wild-type cells, is slow to develop and is not as pronounced. The duration of one cycle of movement for these cells is 60 ± 20 seconds (mean \pm s.d.; $n=9$, in 9 cells). Regions of high traction stress are found at the rear and also along the lateral cell edges (Fig. 5A–E, see supplementary material, Movie 4). In addition these tractions are usually only double the magnitude of traction stresses at the front. In contrast, traction stresses at the rear of wild-type cells are often ten fold greater than at the front. As in wild-type cells, areas of low traction stress are found at the protruding edge but are smaller in magnitude (Fig. 5A–H). In *mlcE*⁻ cells, the asymmetrical pattern of traction stress develops more slowly (~ 40 seconds longer) than in wild-type cells, and accounts for the significant reduction in speed of *mlcE*⁻ cells. In addition, *mlcE*⁻ cells exhibit more slow recoil (77%) retractions than rapid recoil (23%) ones, and the former take significantly longer to complete compared with wild-type cells. For example, it takes ~ 24 seconds for the *mlcE*⁻ cell in Fig. 5 to complete a slow recoil retraction, compared with ~ 15 seconds for the wild-type cell in Fig. 4. Prior to a slow recoil

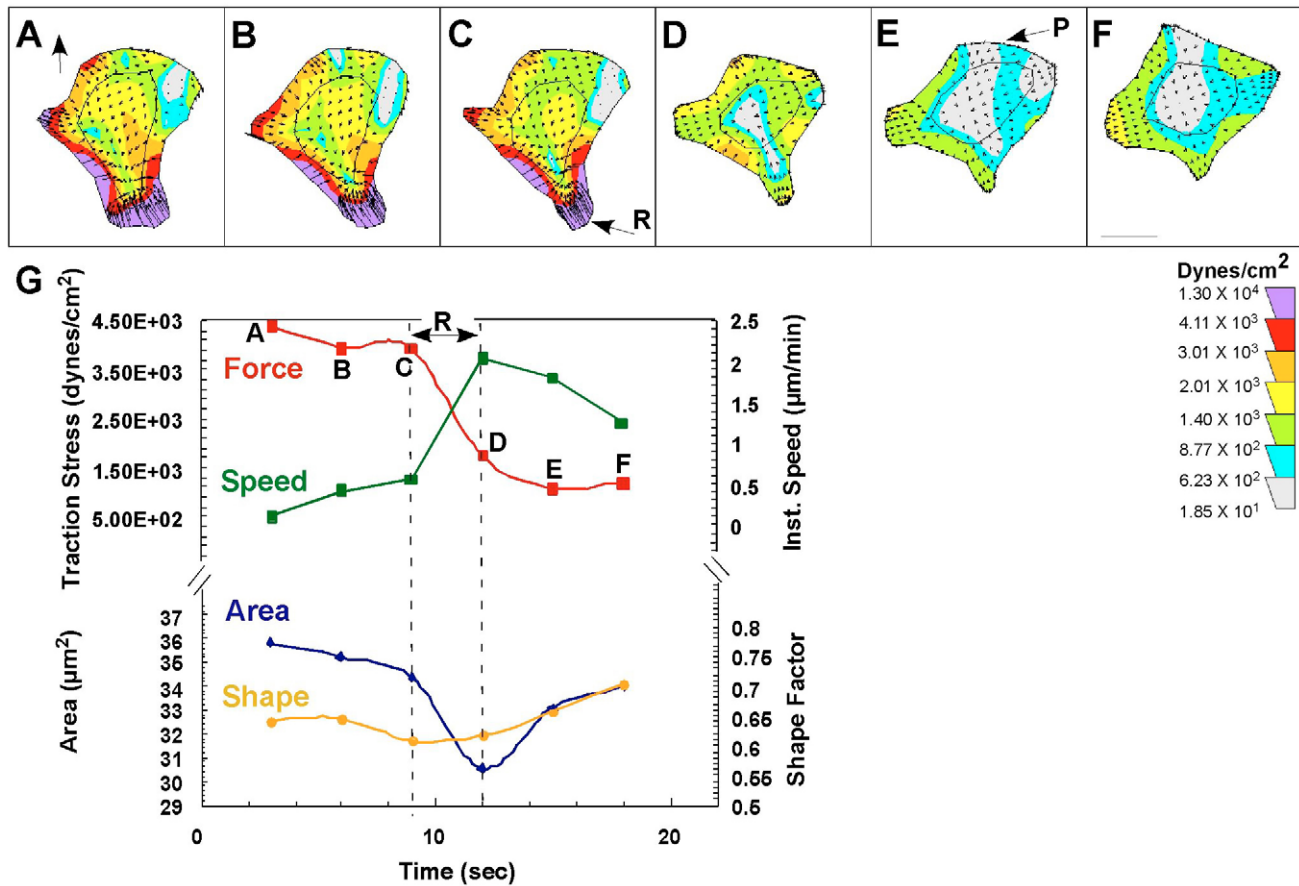


Fig. 3. Changes in distribution of traction stress generated by a wild-type *Dictyostelium* cell during a 'rapid recoil' retraction. (A-F) A time series of traction vector maps obtained from a wild-type cell moving in the general direction indicated (arrow), corresponding to one cycle of movement. The highest 90th percentile traction stresses (red and purple regions) are located in a crescent-shaped region at the rear of the cell (A,B,C) prior to retraction (R in C) at the rear (arrow) then disappear abruptly following retraction (D-F). Regions of low traction stress (white to green regions) are consistently found at the front of the cell (A-F). Once retraction has occurred these regions allow for protrusion to begin (P in E,F). Bar, 3 μm . (G) Plots of the 90th percentile traction stress (red), instantaneous speed (green), cell area (blue) and shape factor (yellow) corresponding to panels A-F. The rapid recoil retraction (R) occurs between ~9-12 seconds (C,D) as indicated by the two vertical dotted lines.

retraction both 90th percentile traction stress and speed increase over a ~27 second period, while the cells become elongated, indicated by the increase in area (Fig. 5A-D,I). This is because protrusion can still occur at the front, even though retraction is impaired. During retraction, 90th percentile traction stress, speed and area decrease, while cell shape becomes more rounded (Fig. 5E-H,I).

An asymmetrical distribution of traction stress rarely develops in *mhcA*⁻ cells

Mutant *mhcA*⁻ cells have the least well-defined cycles of movement compared with wild-type and *mlcE*⁻ cells and virtually all retractions (92%) observed are of the slow recoil type. One cycle of movement for the *mhcA*⁻ cells lasts 28 ± 8 seconds (mean \pm s.d.; $n=5$, in 5 cells). The inability of *mhcA*⁻ cells to become polarized is shown by the occurrence of one or more lateral protrusions and along the cell margin (Fig. 6A-J). In addition, *mhcA*⁻ cells are more spread, reflecting the absence of actin crosslinking activity that would normally stiffen the actin cortex (Laevsky and Knecht, 2003; Pasternak et al., 1989). The *mhcA*⁻ cells have the lowest range of traction

stress and are also stationary for extended periods, during which time a symmetrical distribution of traction stress exists (data not shown). This consists of several regions of 90th percentile traction stress arranged along the cell margin, whose distribution changes rapidly from one frame to the next, giving the cell the appearance of 'jiggling' in place. Occasionally, *mhcA*⁻ cells, including this example, develop a short-lived (~13 seconds, compared with ~26 seconds in wild-type cells) asymmetrical pattern of traction stress (Fig. 6A-I, see supplementary material, Movie 5) that is accompanied by a brief increase in cell speed, which can match the rates of slow-moving wild-type cells (Fig. 6K). During the slow recoil retraction shown here, changes in traction stress, speed, cell area and shape are similar to those observed in wild-type and *mlcE*⁻ cells. Prior to retraction, a region of high traction stress enlarges at the rear, together with a simultaneous rise in 90th percentile traction stress and cell speed (Fig. 6A-E,K). At the onset of retraction, cell area decreases and the cell becomes more rounded as a region of high traction stress encircles most of the cell (Fig. 6E,F). During retraction, both traction stress and cell speed decrease (Fig. 6E-J,K). Meanwhile, an increase

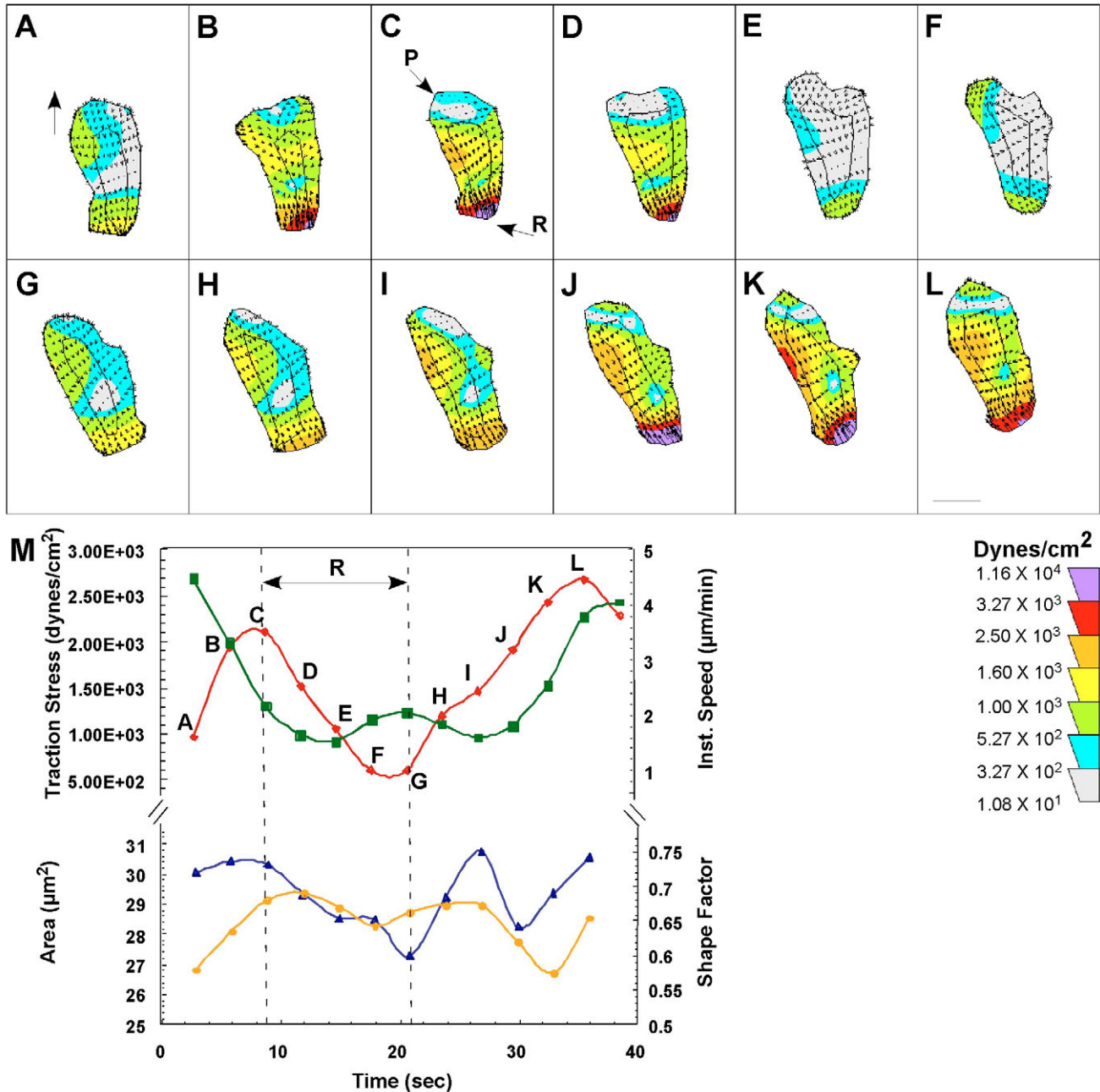


Fig. 4. Changes in distribution of traction stress generated by a wild-type *Dictyostelium* cell during a 'slow recoil' retraction. (A-L) A time series of traction vector maps obtained from a wild-type cell moving in the general direction indicated (arrow). Traction stresses increase gradually (A-C), particularly at the rear (arrow in C), prior to retraction (R in C) and decrease during retraction (C-G). Protrusion (P in C) occurs simultaneously with retraction (C-G) at the front of cell where there are regions of low traction stresses. Bar, 3 μm. (M) Plots of the 90th percentile traction stress (red), instantaneous speed (green), cell area (blue) and shape factor (yellow) corresponding to panels A-L. A-G constitute one cycle of movement that includes the first slow recoil retraction (R) which occurs between 9 and 21 seconds, as indicated by the vertical dotted lines. H-L show the beginning of a second cycle of movement, prior to the onset of a slow recoil retraction (not shown). Note the gradual increase in traction stress at the rear and its similarity to panels A-D.

in cell area and elongation of cell shape occurs, owing to a transient rise in the rate of protrusion (Fig. 6K).

Two additional patterns of traction stress are observed in *mhcA*⁻ cells that are not seen in wild-type cells. The first type, which was also observed in a few *mlcE*⁻ cells (data not shown), consists of high traction stresses at both the front and rear cell edges. During this period no net movement occurs

until retraction or protrusion proceeds at one end. The second pattern of traction stress is only observed for short periods in *mhcA*⁻ cells that generate the lowest range of traction stresses. It consists of a large area of 90th percentile traction stress at the protruding edge together with low traction stresses at the rear, and is accompanied by a brief increase in speed.

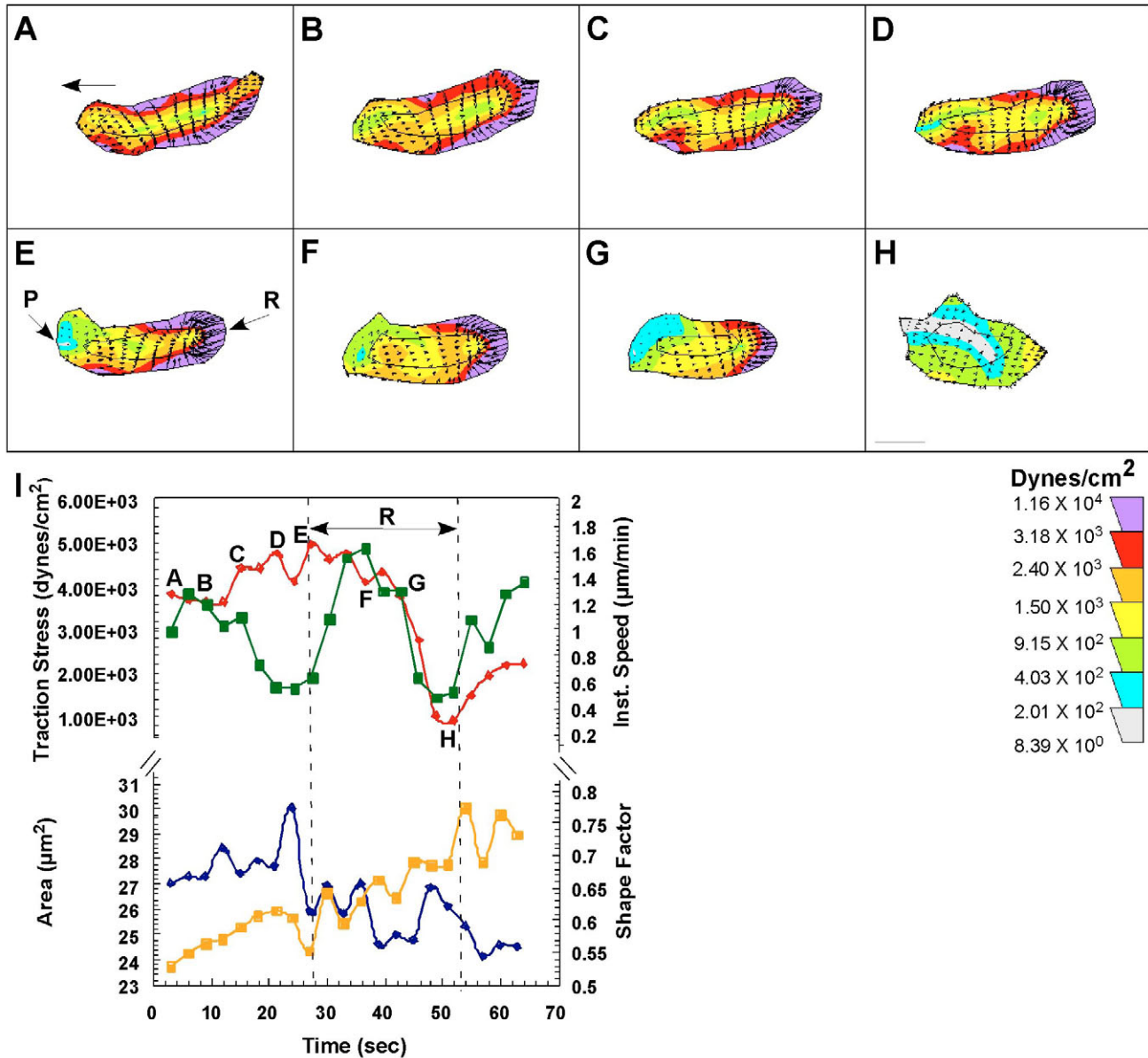


Fig. 5. Changes in distribution of traction stress generated by a *mlcE*⁻ *Dictyostelium* cell during a 'slow recoil' retraction. (A-H) A time series of traction vector maps obtained from a *mlcE*⁻ cell moving in the general direction indicated (arrow), during one cycle of movement. An asymmetrical distribution of high traction stress develops very slowly at the rear and along the lateral cell edges (A,D) prior to retraction (R in E, arrow). During the slow recoil retraction, traction stress decreases gradually together with a progressive loss in front-rear asymmetry (E-H), while protrusion (P in E) is occurring at the cell front, where traction stresses are low. Bar, 3 μm . (I) Plots of the 90th percentile traction stress (red), instantaneous speed (green), cell area (blue) and shape factor (yellow) corresponding to panels A-H. The slow recoil retraction (R) occurs between ~28–52 seconds, as indicated by the vertical dotted lines.

Discussion

We have shown that rapid movement in all *Dictyostelium* cell types studied here is dependent on the development of a front-rear asymmetry in traction stress and not solely on the absolute magnitude of traction stress. In *mlcE*⁻ cells, myosin II actin crosslinking activity tends to stabilize the distribution of traction stresses however, without the myosin II motor activity, traction stress asymmetry is poor and develops slowly, leading to decreased cell speed. The lack of all myosin II function in *mhcA*⁻ cells is related to their inability to develop and maintain an asymmetrical distribution of traction stress and is the major

reason for their reduced speed. We conclude that that cell speed for each cell type is determined by the rate and extent to which traction stress asymmetry develops, and can be related to the distinct roles of myosin II motor and actin crosslinking activity.

The distribution of traction forces, not their magnitude, determines cell speed

There is much evidence to suggest that myosin II is involved in retraction of the rear cell edge (Chen, 1981; Clow and McNally, 1999; Jay et al., 1995). High traction stresses have been found at the rear of fibroblasts and keratocytes where they

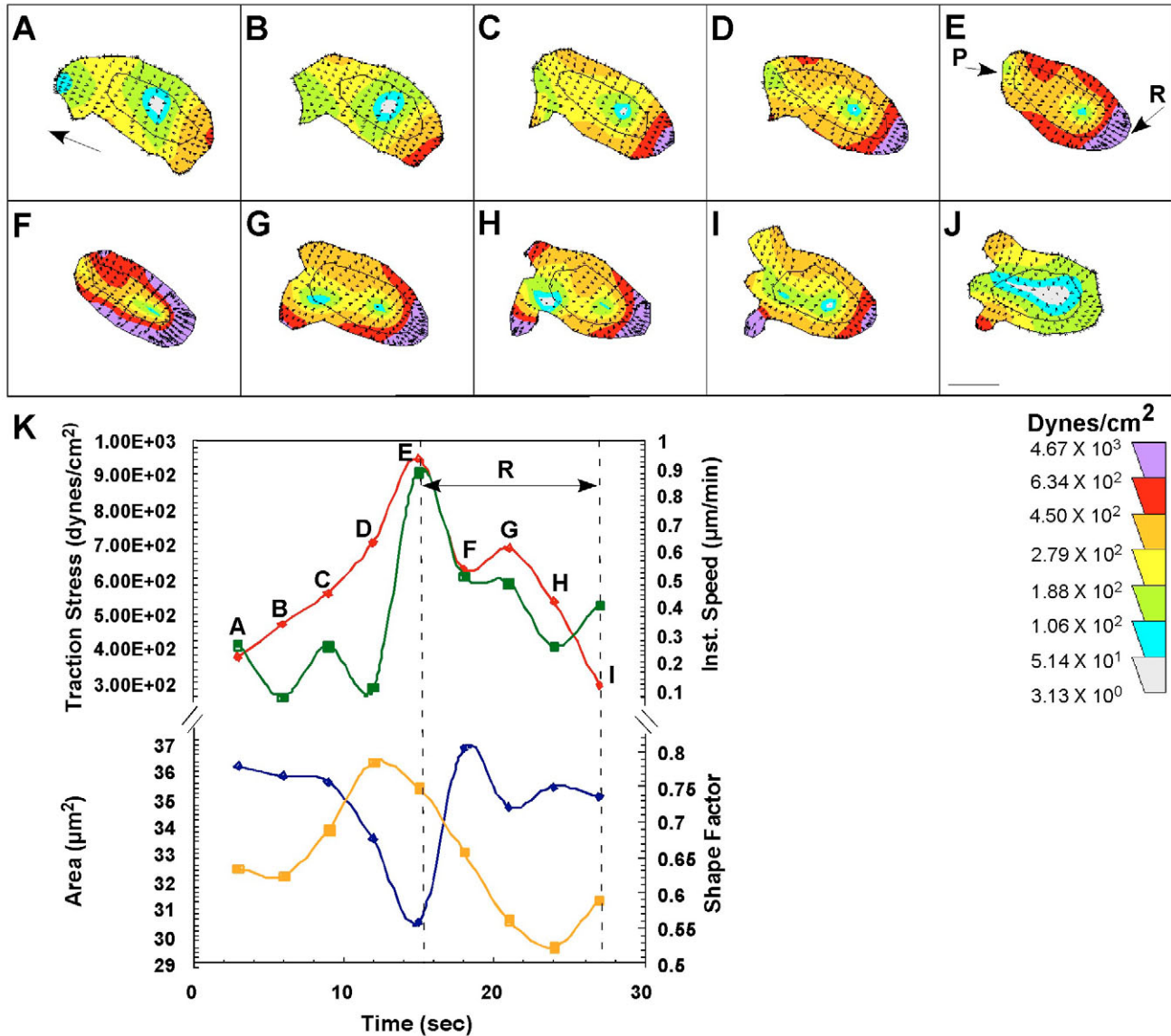


Fig. 6. Changes in distribution of traction stress generated by a *mhca*⁻ *Dictyostelium* cell during a 'slow recoil' retraction. (A-J) A time series of traction vector maps obtained from a *mhca*⁻ cell moving in the general direction indicated (arrow), during one cycle of movement. An asymmetrical distribution of traction stress occurs slowly (A-E), but more rapidly than in *mleE*⁻ cells. Regions of highest 90th percentile traction stress (purple, red) enlarge at the rear and extend along the lateral cell edges. During retraction (R in E) at the rear (arrow) traction stresses gradually decrease, particularly at the rear (E-J), while at the same time protrusion (P in E) is occurring at the front where low tractions are present (E-J). Bar, 3 μm. (K) Plots of the 90th percentile traction stress (red), instantaneous speed (green), cell area (blue), shape factor (yellow) corresponding to panels A-J. The slow recoil retraction (R) occurs between ~15 to 27 seconds, as indicated by the vertical dotted lines. Note that for illustrative purposes the color scale represents a range of magnitudes that is ~25 times less than the one used for the wild-type cells in Figs 3 and 4.

are thought to provide the necessary force to rupture adhesions at the rear (Dembo et al., 1996; Dembo and Wang, 1999; Lee et al., 1994). Although our observations of high traction stresses at the rear of wild-type *Dictyostelium* cells are consistent with this idea, we suggest that these forces may also contribute to cell motility by other means. One possibility is that high tractions at the rear inhibit protrusion, whereas low traction stresses at the front favor protrusion. In support of this, cells lacking myosin II have increased lateral pseudopod formation (Chung and Firtel, 2002). Therefore, we propose that myosin II has a role in the development of an asymmetrical

distribution of traction stress that is essential for rapid, polarized cell movement. In support of this idea, we found that some wild-type cells that generate the highest tractions but do not have an asymmetrical distribution of traction stresses, move very slowly. Conversely, *mhca*⁻ cells that produce very low traction stresses can move as fast as some slower moving wild-type cells, but only for short periods when an asymmetrical distribution of traction stress is present. Presumably, during this time, myosin-II-independent contractile forces, although small, are sufficient to inhibit protrusion at the rear while allowing protrusion at the front. However, the fact that *mhca*⁻

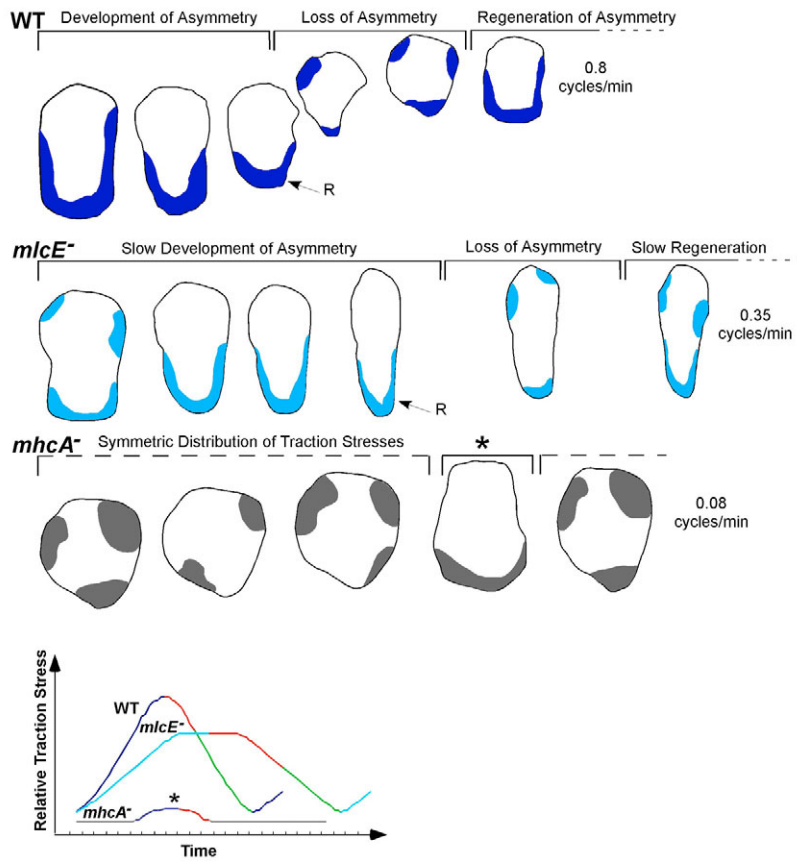


Fig. 7. Diagram of the hypothetical relationship between the spatio-temporal distribution of traction stress and a cycle of movement for each cell type. For each cell type, colored areas represent the average 90th percentile traction stress that is highest for the wild-type (dark blue), intermediate for *mlcE*⁻ (light blue) and very low for *mhcA*⁻ cells (gray). Periods of development, loss and regeneration of traction stress asymmetry are indicated by horizontal bars. The total number of cycles occurring within a period of observation (~3 minutes) is expressed as cycles per minute. Graph illustrating differences in the rate of development (blue), retraction (red) and regeneration (green) of traction stress asymmetry for the wild-type, *mlcE*⁻ and *mhcA*⁻ cells. The gray line represents a period in which *mhcA*⁻ cells lack traction stress asymmetry, except where marked (asterisk).

cells rarely develop an asymmetrical distribution of traction stress is the reason for their slow rate of movement when observed over longer time scales.

We suggest that the higher average traction stress and the inverse relationship between traction stress and cell speed measured in wild-type *Dictyostelium* may be due to their increased adhesiveness, as previously reported for keratocytes (Doyle and Lee, 2005). This is supported by the fact that wild-type *Dictyostelium* cells exhibit more rapid recoil retractions than slow recoil retractions, therefore adhesions at the rear must be strong enough to resist a significant rise in traction stress. Our data suggest that the rise in average 90th percentile traction stress, prior to a rapid recoil retraction also inhibits protrusion at the front because protrusions occur after the rear has detached and traction stress decreases. Conversely, the detachment of weaker adhesions will be associated with slow recoil retractions and less force will be required. The smaller rise in traction stress associated with this type of retraction is

less likely to inhibit protrusion, which is why cell speed and traction stress tend to increase together.

Myosin II motor activity promotes the development of an asymmetrical distribution of traction stress

The observation that myosin II becomes concentrated at the rear of migrating cells (Kolega, 2006; Rubino et al., 1984; Verkhovsky et al., 1999; Yumura et al., 1984) agrees with our hypothesis that myosin II motor activity promotes the development of traction stress asymmetry. Further evidence for this idea comes from studies of cell polarity, where it was shown that a uniform distribution of myosin II exists in apolar keratocyte fragments, but becomes localized at the rear as the fragment develops polarity and begins to move (Svitkina et al., 1997). Furthermore, it was suggested that myosin-II-dependent contractile forces self-organize myosin II to the rear, where it facilitates retraction.

Comparison between patterns of traction stress generated by wild-type and *mlcE*⁻ cells suggests that aggregation of *mlcE*⁻ myosin II toward the rear is impaired. This is reflected by the slow development of traction stress asymmetry in which high traction stresses are not completely localized to the rear. In addition, the magnitude of these tractions are sometimes only double those at the front, in contrast to wild-type cells where there is a tenfold difference in traction magnitude between the front and rear. Consistent with this observation is the finding that in dividing *mlcE*⁻ cells, the cleavage furrow is unable to completely contract, even though the quantity and intracellular localization of myosin II in *mlcE*⁻ cells is similar to that of wild-type cells (Chen et al., 1995). Likewise, the coalescence of myosin II from a 'C' shape to a spot within the actin cortex of cells that lack the myosin II regulatory light chain is much slower than the C-

to-spot transition in wild-type cells (Clow and McNally, 1999). We further suggest that the partial development of traction stress asymmetry in *mlcE*⁻ cells will impede retraction and cell movement because force application at the rear is less focused and significantly lower than in wild-type cells. As a result, retraction may be dependent on the slow rise of tension within the actin cortex (Laevsky and Knecht, 2003) or the eventual dissociation of *mlcE*⁻ myosin II from F-actin at the cell rear.

Myosin II motor and actin crosslinking activity are both required to develop and maintain asymmetrical patterns of traction stress

The role of myosin II actin crosslinking activity is apparent from the comparison of traction stress patterns generated by *mlcE*⁻ and *mhcA*⁻ cells. The inability of *mhcA*⁻ cells to maintain a stable pattern of traction stresses is in stark contrast to *mlcE*⁻ cells and clearly implicates myosin II actin crosslinking

activity in stabilizing the distribution of traction stress. In addition, the ability of *mlcE*⁻ cells to generate traction stresses that are significantly greater in magnitude than *mhca*⁻ cells, suggests that *mlcE*⁻ myosin II actin crosslinking activity may generate contractile forces, possibly because of some residual motor activity or by increasing the rigidity of the actin cortex (Xu et al., 2001).

The fact that some *mhca*⁻ cells can develop polarity, even for a shorter duration, suggests that these cells can develop and maintain an asymmetrical distribution of traction stresses in a myosin-II-independent manner. One possible explanation is that myosin II function may be compensated by other actin-binding proteins in the *mhca*⁻ cells. For example, there is evidence to suggest that the knockout of myosin II may be recovered by overexpression of other actin crosslinkers that form stronger bonds with actin than myosin II (Merkel et al., 2000). Another possibility is that unconventional myosin motors, such as myosin I (Condeelis, 1992; Dai et al., 1999; Fukui et al., 1989; Titus, 1993; Wessels et al., 1996) may contribute to the development of traction stress asymmetry and the movement of *mhca*⁻ cells. Actin filament dynamics may also play a role in generating an asymmetrical distribution of traction stresses, since cortical actin flow has been shown to be independent of myosin II but occurs at a slower rate than in wild-type cells (Jay and Elson, 1992).

We propose that the kinetics of myosin II association with actin filaments, force production and dissociation from F-actin at the rear, drives cycles of movement that include the development and regeneration of traction stress asymmetry (Fig. 7). In addition, we suggest that the rate at which traction stress asymmetry develops and is regenerated following retraction has a very important influence on cell speed because it determines the duration and frequency of cycles of movement. We believe that myosin II motor and actin-crosslinking activity act synergistically to reduce the duration and increase the frequency of cycles of movement in wild-type *Dictyostelium*. For example, in wild-type cells, where retractions are generally of the rapid recoil type, cycle duration is relatively short and on average we observe one cycle every 1.25 minutes, which is similar to that found for cAMP-responsive wild-type *Dictyostelium* (Wessels et al., 1998). By contrast, we observe one cycle every ~12 minutes for *mhca*⁻ cells. In wild-type cells, myosin II is an active actin crosslinker that can associate and dissociate very rapidly in the presence of ATP (Prassler et al., 1997). Thus upon myosin II actin crosslinking, the generation of force will cause myosin-actin complexes to aggregate toward the rear, whereas actin crosslinking will stabilize them. This allows the development of an asymmetrical distribution of traction stresses to occur more rapidly than in *mlcE*⁻ cells, which exhibit one cycle of movement every 3 minutes. Furthermore, it is possible that in addition to providing force for cell detachment, myosin II motor activity facilitates retraction at the rear by increasing the dissociation rate of myosin II from actin (Verkhovskiy et al., 1999). We hypothesize that following a brief loss in traction stress asymmetry during retraction, the re-association of myosin II with actin allows traction stress asymmetry to regenerate, thus initiating another cycle of movement. Without motor activity, traction stress asymmetry cannot develop as efficiently in *mlcE*⁻ cells as in wild-type cells, and this lengthens the cycle of movement. In addition, we suggest that

the dissociation rate of *mlcE*⁻ myosin II from actin is also reduced, which may slow the rate of retraction. Thus the slow development and regeneration of traction stress asymmetry in *mlcE*⁻ cells can explain why the average speed of these cells is the same as *mhca*⁻ cells, even though they generate traction stresses around seven times greater. Therefore, the absence of myosin II motor and actin-crosslinking activities can account for our observation that the development of traction stress asymmetry is rare and short-lived in *mhca*⁻ cells.

Materials and Methods

Cell lines and cultures

All *Dictyostelium discoideum* cell lines were grown in 100-mm plastic Petri dishes with 10 ml HL-5 nutrient medium (Sussman and Sussman, 1967). NC4A2 is a spontaneous axenic derivative of wild-type NC4 (Knecht and Sheldon, 1995; Morrison and Harwood, 1992). HK321 is a myosin heavy chain null mutant (*mhca*⁻) derived from NC4A2 (Shelden and Knecht, 1995). *mlcE*⁻ is an essential light chain null mutant, generated by targeted disruption (Chen et al., 1995). The *mlcE*⁻ myosin II has little or no motor activity but can crosslink actin. *MlcE*⁺ is used as a wild-type control for the *mlcE*⁻ cells. This cell line was constructed by integrating the essential light chain gene back into the genome of *mlcE*⁻ cells driving expression with an actin promoter (Chen et al., 1995; Pollenz et al., 1992).

Manufacture and calibration of gelatin substrata

The gelatin substrata were manufactured and calibrated as previously described (Doyle and Lee, 2002). Stock gels were made with 2.5% gelatin (Nabisco, Parsippany, NJ) dissolved in HL-5 medium. Before use, the gel was liquefied at 40°C and a 400 µl aliquot was transferred into a Rappaport chamber and allowed to solidify at 4°C. Orange microspheres, diluted at a concentration of 1:100 (0.2 µm, Bangs Laboratories, Fishers, IN) in distilled water, were then added to the gelatin and the excess bead solution was aspirated off immediately. The remaining bead solution was allowed to dry onto the gelatin for 1 hour at 4°C, then briefly (~10 seconds) warmed on a hot plate to liquefy the lower layer of the gelatin. After removal from the hot plate, ~330 µl of the gelatin solution was carefully removed from the bottom of the chamber using a small pipette tip, being careful not to disturb the surface. Gels were then rapidly cooled for 30 seconds by placing cell chambers on a level metal sheet, pre-cooled to -20°C. This produced a thin layer of gelatin about 40 µm thick whose top surface was embedded with a monolayer of fluorescent beads.

Calibration of gelatin substrata was performed by placing a steel ball (diameter, 0.3 mm; density, 14.95 g/cm³; Hoover Precision, East Granby, CT) on the substratum and measuring the resulting surface indentation. The Young's Modulus (Y) is given by: $Y = 3(1 - \nu^2) / 4d^{3/2}r^{1/2}$, where ν is the Poisson ratio (assumed here to be 0.3), f is the force applied by the steel ball, d is the size of the indentation, and r is the bead radius. The Young's Modulus for the gelatin substrata used in this study is ~2.5 kPa with a range of ±10%. Measurements were made in five random locations and the average value for d was used to calculate the Young's Modulus for each substratum.

Dual image microscopy

Dictyostelium cells were harvested in HL-5 medium and the concentration was adjusted to 1 × 10⁶ cells/ml. A 500 µl cell suspension was then added to the Rappaport chambers and the cells were allowed to adhere to the gelatin for 3 minutes, after which the medium was removed and replaced with 1 ml of fresh HL-5 medium. The cells were incubated for at least 2 hours at 22°C before imaging.

A DIC image of the cell and a fluorescence image (excitation at 560 nm) of the marker beads embedded within the gelatin, were collected simultaneously, using a Leica TCS SP2 confocal microscope system (Leica Microsystems, Heidelberg, Germany) with a Plan APO, 100× 1.4 NA oil objective. Pairs of 512 × 512 pixel images were acquired every 3.3 seconds. See supplementary material, Movie 1.

Measurement of substratum deformation and generation of traction maps

A vector map of substratum deformation was generated for each time point using an image of beads in their displaced positions and another reference or null image of beads in their undisplaced positions, after the cell has moved away. Substratum deformation was calculated by comparing the positions of marker beads between the displaced and reference images, using a correlation-based optical flow algorithm (Dembo and Wang, 1999; Marganski et al., 2003). Custom software (LIBTRC) was then used for calculating and generating traction vector maps as previously described (Dembo and Wang, 1999). Briefly, a traced cell outline was used as a guide to generate a mesh of approximately 200 quadrilateral elements to form the interior of the cell. The most likely traction vector at each node of this mesh was estimated by fitting the displacement data, using the formulae of Boussinesque.

Morphometric analysis

Diagrams of stacked cell outlines with an overlaid track of the cell centroid were generated using DIAS 3.0 (The Dynamic Image Analysis System, Solltech, Oakdale, IA (Soll et al., 2003)). Rose plots were obtained by plotting the x , y coordinates of the cell centroid, after setting the coordinates of the initial position to zero. Morphometric analysis of cell speed, area and shape factor was performed using Metamorph analysis software (Universal Imaging, West Chester, PA) for nine cells of each type moving approximately one body length. Instantaneous cell speed was calculated by dividing the distance between each centroid by the corresponding time period (3 seconds). These data were smoothed using a running average of three. Shape factor was measured for each time point using the following equation, Shape factor = $(4\pi \times A)/P^2$, where A is cell area and P is cell perimeter. A running average of three was used to smooth the cell shape and area data. Persistence was calculated by dividing the net cell displacement by the total displacement. In Fig. 1D-F, the average percent change in measures of instantaneous speed, persistence and area was calculated with respect to the wild-type value that was set to 100%.

To relate changes in distribution of traction stress to cell movement, the 90th percentile traction force was plotted against cell speed, area and shape for each cell. The 90th percentile value was used because it provides a more sensitive measure of changes in traction stress than either the average traction stress, which is sensitive to the spread area of the cell, or the maximal traction stress, which is more sensitive to noise in the data.

The work was supported by a National Science Foundation Grant MCB-0114231 to J.L. and a NIH grant GM-40590 to D.A.K.

References

- Beningo, K. A. and Wang, Y. L. (2002). Flexible substrata for the detection of cellular traction forces. *Trends Cell Biol.* **12**, 79-84.
- Beningo, K. A., Lo, C. M. and Wang, Y. L. (2002). Flexible polyacrylamide substrata for the analysis of mechanical interactions at cell-substratum adhesions. *Methods Cell Biol.* **69**, 325-339.
- Burton, K., Park, J. H. and Taylor, D. L. (1999). Keratocytes generate traction forces in two phases. *Mol. Biol. Cell* **10**, 3745-3769.
- Chen, T.-L., Kowalczyk, P. A., Ho, G. and Chisholm, R. L. (1995). Targeted disruption of the Dictyostelium myosin essential light chain gene produces cells defective in cytokinesis and morphogenesis. *J. Cell Sci.* **108**, 3207-3218.
- Chen, W. T. (1981). Mechanism of retraction of the trailing edge during fibroblast movement. *J. Cell Biol.* **90**, 187-200.
- Chung, C. Y. and Firtel, R. A. (2002). Signaling pathways at the leading edge of chemotaxing cells. *J. Muscle Res. Cell Motil.* **23**, 773-779.
- Clow, P. A. and McNally, J. G. (1999). In vivo observations of myosin II dynamics support a role in rear retraction. *Mol. Biol. Cell* **10**, 1309-1323.
- Condeelis, J. (1992). Are all pseudopods created equal? *Cell Motil. Cytoskeleton* **22**, 1-6.
- Dai, J., Ting-Beall, H. P., Hochmuth, R. M., Sheetz, M. P. and Titus, M. A. (1999). Myosin I contributes to the generation of resting cortical tension. *Biophys. J.* **77**, 1168-1176.
- Dembo, M. and Wang, Y. L. (1999). Stresses at the cell-to-substrate interface during locomotion of fibroblasts. *Biophys. J.* **76**, 2307-2316.
- Dembo, M., Oliver, T., Ishihara, A. and Jacobson, K. (1996). Imaging the traction stresses exerted by locomoting cells with the elastic substratum method. *Biophys. J.* **70**, 2008-2022.
- Doolittle, K. W., Reddy, I. and McNally, J. G. (1995). 3D analysis of cell movement during normal and myosin-II-null cell morphogenesis in Dictyostelium. *Dev. Biol.* **167**, 118-129.
- Doyle, A. D. and Lee, J. (2002). Simultaneous, real-time imaging of intracellular calcium and cellular traction force production. *Biotechniques* **33**, 358-364.
- Doyle, A. D. and Lee, J. (2005). Cyclic changes in keratocyte speed and traction stress arise from Ca^{2+} -dependent regulation of cell adhesiveness. *J. Cell Sci.* **118**, 369-379.
- Fukui, Y., Lynch, T. J., Brzeska, H. and Korn, E. D. (1989). Myosin I is located at the leading edges of locomoting Dictyostelium amoebae. *Nature* **341**, 328-331.
- Harris, A. K., Wild, P. and Stopak, D. (1980). Silicone rubber substrata: a new wrinkle in the study of cell locomotion. *Science* **208**, 177-179.
- Ho, G. and Chisholm, R. L. (1997). Substitution mutations in the myosin essential light chain lead to reduced actin-activated ATPase activity despite stoichiometric binding to the heavy chain. *J. Biol. Chem.* **272**, 4522-4527.
- Jay, P. Y. and Elson, E. L. (1992). Surface particle transport mechanism independent of myosin II in Dictyostelium. *Nature* **356**, 438-440.
- Jay, P. Y., Pham, P. A., Wong, S. A. and Elson, E. L. (1995). A mechanical function of myosin II in cell motility. *J. Cell Sci.* **108**, 387-393.
- Knecht, D. A. and Sheldon, E. (1995). Three-dimensional localization of wild-type and myosin II mutant cells during morphogenesis of dictyostelium. *Dev. Biol.* **170**, 434-444.
- Kolega, J. (2006). The role of myosin II motor activity in distributing myosin asymmetrically and coupling protrusive activity to cell translocation. *Mol. Biol. Cell* **17**, 4435-4445.
- Laevsky, G. and Knecht, D. A. (2003). Cross-linking of actin filaments by myosin II is a major contributor to cortical integrity and cell motility in restrictive environments. *J. Cell Sci.* **116**, 3761-3770.
- Lee, J., Leonard, M., Oliver, T., Ishihara, A. and Jacobson, K. (1994). Traction forces generated by locomoting keratocytes. *J. Cell Biol.* **127**, 1957-1964.
- Marganski, W. A., Dembo, M. and Wang, Y. L. (2003). Measurements of cell-generated deformations on flexible substrata using correlation-based optical flow. *Meth. Enzymol.* **361**, 197-211.
- Merkel, R., Simson, R., Simson, D. A., Hohenadl, M., Boulbitch, A., Wallraff, E. and Sackmann, E. (2000). A micromechanic study of cell polarity and plasma membrane cell body coupling in Dictyostelium. *Biophys. J.* **79**, 707-719.
- Morrison, A. and Harwood, A. (1992). A simple method of generating axenic derivatives of Dictyostelium strains. *Exp. Cell Res.* **199**, 383-386.
- Munevar, S., Wang, Y. L. and Dembo, M. (2001). Distinct roles of frontal and rear cell-substrate adhesions in fibroblast migration. *Mol. Biol. Cell* **12**, 3947-3954.
- Oliver, T., Jacobson, K. and Dembo, M. (1998). Design and use of substrata to measure traction forces by cultured cells. *Meth. Enzymol.* **298**, 497-521.
- Pasternak, C., Spudich, J. A. and Elson, E. L. (1989). Capping of surface receptors and concomitant cortical tension are generated by conventional myosin. *Nature* **341**, 549-551.
- Pollenz, R. S., Chen, T.-L. L., Trivinos-Lagos, L. and Chisholm, R. L. (1992). The dictyostelium essential light chain is required for myosin function. *Cell* **69**, 951-962.
- Prassler, J., Stocker, S., Marriott, G., Heidecker, M., Kellermann, J. and Gerisch, G. (1997). Interaction of a Dictyostelium member of the plastin/fimbrin family with actin filaments and actin-myosin complexes. *Mol. Biol. Cell* **8**, 83-95.
- Rubino, S., Fighetti, M., Unger, E. and Cappuccinelli, P. (1984). Location of actin, myosin, and microtubular structures during directed locomotion of Dictyostelium amoebae. *J. Cell Biol.* **98**, 382-390.
- Shelden, E. and Knecht, D. A. (1995). Mutants lacking myosin II cannot resist forces generated during multicellular morphogenesis. *J. Cell Sci.* **108**, 1105-1115.
- Soll, D. R., Wessels, D., Heid, P. J. and Voss, E. (2003). Computer-assisted reconstruction and motion analysis of the three-dimensional cell. *ScientificWorldJournal* **3**, 827-841.
- Sussman, R. and Sussman, M. (1967). Cultivation of Dictyostelium discoideum in axenic medium. *Biochem. Biophys. Res. Commun.* **29**, 53-55.
- Svitkina, T. M., Verkhovskiy, A. B., McQuade, K. M. and Borisy, G. G. (1997). Analysis of the actin-myosin II system in fish epidermal keratocytes: mechanism of cell body translocation. *J. Cell Biol.* **139**, 397-415.
- Titus, M. A. (1993). Myosins. *Curr. Opin. Cell Biol.* **5**, 77-81.
- Uchida, K. S., Kitanishi-Yumura, T. and Yumura, S. (2003). Myosin II contributes to the posterior contraction and the anterior extension during the retraction phase in migrating Dictyostelium cells. *J. Cell Sci.* **116**, 51-60.
- Verkhovskiy, A. B., Svitkina, T. M. and Borisy, G. G. (1999). Self-polarization and directional motility of cytoplasm. *Curr. Biol.* **9**, 11-20.
- Wessels, D., Soll, D. R., Knecht, D., Loomis, W. F., De Lozanne, A. and Spudich, J. (1988). Cell motility and chemotaxis in Dictyostelium amoebae lacking myosin heavy chain. *Dev. Biol.* **128**, 164-177.
- Wessels, D., Titus, M. and Soll, D. R. (1996). A Dictyostelium myosin I plays a crucial role in regulating the frequency of pseudopods formed on the substratum. *Cell Motil. Cytoskeleton* **33**, 64-79.
- Wessels, D., Voss, E., Von Bergen, N., Burns R., Stites, J. and Soll, D. R. (1998). A computer-assisted system for reconstructing and interpreting the dynamic three-dimensional relationships of the outer surface, nucleus and pseudopods of crawling cells. *Cell Motil. Cytoskeleton* **41**, 225-246.
- Xu, X. S., Lee, E., Chen, T.-L., Kuczmariski, E., Chisholm, R. L. and Knecht, D. A. (2001). During multicellular migration, myosin II serves a structural role independent of its motor function. *Dev. Biol.* **232**, 255-264.
- Yumura, S., Mori, H. and Fukui, Y. (1984). Localization of actin and myosin for the study of amoeboid movement in Dictyostelium using improved immunofluorescence. *J. Cell Biol.* **99**, 894-899.